Supplement of Atmos. Chem. Phys., 20, 2513–2532, 2020
https://doi.org/10.5194/acp-20-2513-2020-supplement

Atmospheric Chemistry and Physics
Open Access

Supplement of

Molecular compositions and optical properties of dissolved brown carbon in biomass burning, coal combustion, and vehicle emission aerosols illuminated by excitation–emission matrix spectroscopy and Fourier transform ion cyclotron resonance mass spectrometry analysis

Jiao Tang et al.

Correspondence to: Jun Li (junli@gig.ac.cn) and Gan Zhang (zhanggan@gig.ac.cn)

Contents:

S1. Data analysis.

Emission factors

Fuel-based emission factors were obtained by the carbon mass balance formula:(Cui et al., 2018;Cui et al., 2017)

$$\mathrm{EF}_i = \frac{\Delta X_i}{\Delta CO_2} \cdot \frac{M_i}{M_{CO_2}} \cdot EF_{CO_2} \quad (1)$$

Here, EF_i and EF_{CO_2}(g kg^{-1} fuel) are the emission factor for species *i* and CO_2, respectively. ΔX_i and ΔCO_2 (mol m^{-3}), as well as M_i and M_{CO_2}(g mol^{-1}) are the background-corrected concentrations and molecular weights of species *i* and CO_2, respectively.

Among the above formula, the CO_2 emission factor (EF_{CO_2}) were calculated as:

$$EF_{CO_2} = \frac{C_F}{c(C_{CO}) + c(C_{CO_2}) + c(C_{PM})} \cdot c(CO_2) \cdot M_{CO_2} \quad (2)$$

Here, C_F (g C kg^{-1} fuel) are the mass of carbon in 1kg fuel; $c(C_{CO})$, $c(C_{CO_2})$ and $c(C_{PM})$ (g C m^{-3}) are the corresponding flue gas mass concentrations of carbon, respectively; $c(CO_2)$ (mol m^{-3}) is the molar concentration of CO_2. Because the CO sensor did not function well in field sampling, here we introduced modified combustion efficiency (MCE) defined as $CO_2/(CO_2+CO)$ as an index of the relative amount of flaming and smoldering combustion occurring during a fire (Ward et al., 1993; Yokelson et al., 1997). Our previous study reported that the MCE of BB with an average value of 0.91 ± 0.07, is acceptable for calculating the CO concentration (Cui et al., 2018 and references therein), and this method was used in this study.

ESI FT-ICR MS data processing

Custom software was applied to calculate all mathematically possible formulas for all ions with a signal-to-noise ratio > 10 using a mass tolerance of ± 1.5 ppm as described elsewhere (Mo et al., 2018;Lin et al., 2015). Formula calculator was performed using the following constraints: C ≤ 45, H ≤ 60, O ≤ 20, N ≤ 3, and S ≤ 2.

Identified formulas with isotopomers (i.e., ^{13}C, ^{18}O, or ^{34}S) were not discussed in this paper. These identified molecular formulas were classified into four main compound groups based on their composition: CHO, CHON, CHOS, and CHONS compounds. For the chemical formula $C_cH_hO_oN_nS_s$, the double bonds equivalent (DBE) used as measure of unsaturated level in a molecule was calculated using the following equation: DBE = (2c + 2 – h + n)/2, and an modified aromaticity index (AI_{mod}) used to estimate the fraction of aromatic and condensed aromatic structures was calculated to estimate the fraction of aromatic and condensed aromatic structures from the formula: AI_{mod} = (1 + c – 0.5o – s – 0.5h)/(c – 0.5o – s – n) (Song et al., 2018;Koch and Dittmar, 2006). Commonly, formulas are as follows: no aromatic ($AI_{mod} < 0.5$), aromatic ($AI_{mod} > 0.5$) and condensed aromatic ($AI_{mod} \geq 0.67$). The van Krevelen (VK) diagram was a useful tool which could provide a visual graphic display of compound distribution (Lv et al., 2016).

From the molecular formula assignments, the intensity-averaged calculations for each sample can be determined by the following equations:(Mo et al., 2018;Song et al., 2018;Lv et al., 2016)

$$O/C_w = \Sigma(w_i * o_i) / \Sigma(w_i * c_i) \quad (3)$$

$$H/C_w = \Sigma(w_i * hi) / \Sigma(w_i * c_i) \quad (4)$$

$$DBE_w = \Sigma(w_i * DBE_i) / \Sigma w_i \quad (5)$$

$$AI_{mod,w} = \Sigma(w_i * AI_{mod,i}) / \Sigma w_i \quad (6)$$

Where, w_i is the relative abundance for each individual molecular formula, *i*.

S2. Quality control

In this study, the field blank values of TC (TC=OC+EC), WSOC, and MSOC for ambient blank sample were 0.75 ± 0.02 μg C cm^{-2}, 1.2 ± 0.21 μg C cm^{-2}, 0.48 μg C cm^{-2}, respectively. The standard deviation of parallel experiments based on smoke particle samples were 0.01 μg C cm^{-2}, 0.14 μg C mL^{-1}, 0.16 μg C mL^{-1} for TC, WSOC, and MSOC, respectively. We also corrected the procedural blank concentrations of WSOC and MSOC in each sample. The total recoveries of WSOC and MSOC to OC were 112 % ± 14 % for biomass burning, 101 % ± 20 % for coal combustion, and 100 %

± 26 % for vehicle emission.

The value of absorbance for field blank samples at 365 nm was 0.0009 ± 0.00008, much less than that of smoke samples. The standard deviation of parallel experiments of absorbance at 365 nm for instrument and method were 0.00006 and 0.0008, respectively. Further, no obvious peak was found in the fluorescence spectrum of field blank samples. The fluorescence spectrum of samples was measured with their absorbance lower than 1.

Reference:

Chen, Y., Ge, X., Chen, H., Xie, X., Chen, Y., Wang, J., Ye, Z., Bao, M., Zhang, Y., and Chen, M.: Seasonal light absorption properties of water-soluble brown carbon in atmospheric fine particles in Nanjing, China, Atmos. Environ., 230-240, https://doi.org/10.1016/j.atmosenv.2018.06.002, 2018.

Cheng, Y., He, K. B., Zheng, M., Duan, F. K., Du, Z. Y., Ma, Y. L., Tan, J. H., Yang, F. M., Liu, J. M., Zhang, X. L., Weber, R. J., Bergin, M. H., and Russell, A. G.: Mass absorption efficiency of elemental carbon and water-soluble organic carbon in Beijing, China, Atmos. Chem. Phys., 11, 11497-11510, 10.5194/acp-11-11497-2011, 2011.

Cui, M., Chen, Y., Feng, Y., Li, C., Zheng, J., Tian, C., Yan, C., and Zheng, M.: Measurement of PM and its chemical composition in real-world emissions from non-road and on-road diesel vehicles, Atmos. Chem. Phys., 17, 6779-6795, https://doi.org/10.5194/acp-17-6779-2017, 2017.

Cui, M., Chen, Y., Zheng, M., Li, J., Tang, J., Han, Y., Song, D., Yan, C., Zhang, F., Tian, C., and Zhang, G.: Emissions and characteristics of particulate matter from rainforest burning in the Southeast Asia, Atmos. Environ., 191, 194-204, https://doi.org/10.1016/j.atmosenv.2018.07.062, 2018.

Fan, X., Wei, S., Zhu, M., Song, J., Peng, P., amp, apos, and an: Comprehensive characterization of humic-like substances in smoke $PM_{2.5}$ emitted from the combustion of biomass materials and fossil fuels, Atmos. Chem. Phys., 16, 13321-13340, 10.5194/acp-16-13321-2016, 2016.

Koch, B., and Dittmar, T.: Koch, B. P. & Dittmar, T. From mass to structure: An aromaticity index for high-resolution mass data of natural organic matter. Rapid Commun. Mass Spectrom. 20, 926-932, Rapid Commun. Mass Spectrom., 20, 926-932, 10.1002/rcm.2386, 2006.

Li, M., Fan, X., Zhu, M., Zou, C., Song, J., Wei, S., Jia, W., and Peng, P.: Abundances and light absorption properties of brown carbon emitted from residential coal combustion in China, Environ. Sci. Technol., 53, 595-603, https://doi.org/10.1021/acs.est.8b05630, 2018.

Lin, P., Laskin, J., Nizkorodov, S. A., and Laskin, A.: Revealing Brown Carbon Chromophores Produced in Reactions of Methylglyoxal with Ammonium Sulfate, Environ. Sci. Technol., 49, 14257-14266, https://doi.org/10.1021/acs.est.5b03608, 2015.

Liu, J., Mo, Y., Ding, P., Li, J., Shen, C., and Zhang, G.: Dual carbon isotopes ((14)C and (13)C) and optical properties of WSOC and HULIS-C during winter in Guangzhou, China, Sci. Total Environ., 633, 1571-1578, https://doi.org/10.1016/j.scitotenv.2018.03.293, 2018.

Lv, J., Zhang, S., Wang, S., Luo, L., Cao, D., and Christie, P.: Molecular-Scale Investigation with ESI-FT-ICR-MS on Fractionation of Dissolved Organic Matter Induced by Adsorption on Iron Oxyhydroxides, Environ. Sci. Technol., 50, 2328-2336, https://doi.org/10.1021/acs.est.5b04996, 2016.

Mo, Y., Li, J., Jiang, B., Su, T., Geng, X., Liu, J., Jiang, H., Shen, C., Ding, P., Zhong, G., Cheng, Z., Liao, Y., Tian, C., Chen, Y., and Zhang, G.: Sources, compositions, and optical properties of humic-like substances in Beijing during the 2014 APEC summit: Results from dual carbon isotope and Fourier-transform ion cyclotron resonance mass spectrometry analyses, Environ. Pollut., 239, 322-331, https://doi.org/10.1016/j.envpol.2018.04.041, 2018.

Park, S. S., and Yu, J.: Chemical and light absorption properties of humic-like substances from biomass burning emissions under controlled combustion experiments, Atmos. Environ., 136, 114-122, https://doi.org/10.1016/j.atmosenv.2016.04.022, 2016.

Patriarca, C., Bergquist, J., Sjoberg, P. J. R., Tranvik, L., and Hawkes, J. A.: Online HPLC-ESI-HRMS Method for the Analysis and Comparison of Different Dissolved Organic Matter Samples, Environ. Sci. Technol., 52, 2091-2099, https://doi.org/10.1021/acs.est.7b04508, 2018.

Song, J., Li, M., Jiang, B., Wei, S., Fan, X., and Peng, P.: Molecular Characterization of Water-Soluble Humic like Substances in Smoke Particles Emitted from Combustion of Biomass Materials and Coal Using Ultrahigh-Resolution Electrospray Ionization Fourier Transform Ion Cyclotron Resonance Mass Spectrometry, Environ. Sci. Technol., 52, 2575-2585, https://doi.org/10.1021/acs.est.7b06126, 2018.

Ward, D. E.; Radke, L. F.: Emissions measurements from vegetation fires: A comparative evaluation of methods and results. In: Crutzen, P. J.; Goldammer, J. G., eds. Fire in the Environment: The Ecological, Atmospheric, and Climatic Importance of Vegetation Fires. Dahlem Workshop Reports: Environmental Sciences Research Report 13. Chischester, England: John Wiley & Sons. p. 53-76, 1993.

Yan, C., Zheng, M., Sullivan, A. P., Bosch, C., Desyaterik, Y., Andersson, A., Li, X., Guo, X.,

Zhou, T., Gustafsson, Ö., and Collett, J. L.: Chemical characteristics and light-absorbing property of water-soluble organic carbon in Beijing: Biomass burning contributions, Atmos. Environ., 121, 4-12, https://doi.org/10.1016/j.atmosenv.2015.05.005, 2015.

Yokelson, R.J., Susott, R., Ward, D.E., Reardon, J., Griffith, D.W.T.: Emissions from smoldering combustion of biomass measured by open-path Fourier transform infrared spectroscopy. J. Geophys. Res.-Atmos, 102, 18865-18877, https://doi.org/10.1029/97JD00852, 1997.

Table S1. Elemental analysis of 27 main biomass types.

Sample IDs	Latin name	Biomass types			
		N%	C%	H%	O%
1	Eupatorium odoratum L.	0.97	42	6.0	39
2	Chaetocarpus castanocarpus	1.9	46	5.7	41
3	Cassia siamea Lam.	2.3	38	5.5	33
4	Baccaurea ramiflora Lour.	1.5	48	6.3	46
5	Rauvolfieae verticillata*	0.32	49	6.0	46
6	Macaranga denticulata	0.91	49	6.4	46
7	Toona ciliata M. Roem.	0.51	43	7.1	44
8	Duabanga grandiflora	0.46	44	5.8	45
9	Paramichelia baillonii	0.00	48	6.1	49
10	Bischofia polycarpa	0.38	48	6.7	45
11	Rauvolfieae verticillata	0.78	48	6.2	47
12	Pseudostachyum polymorphum	0.71	44	6.6	47
13	Broussonetia papyrifera	0.65	49	7.3	48
14	Citrus maxima	0.66	51	5.7	45
15	Litchi chinensis Sonn.	0.62	46	6.3	44
16	Anthocephalus chinensis	1.6	45	5.7	44
17	Antiaris toxicaria Lesch.	1.0	46	5.9	47
18	Musa nana Lour.	0.86	50	6.8	46
19	Melia azedarach	0.69	47	5.8	48
20	Pterospermum menglunense Hsue	0.72	46	5.3	56
21	Castanopsis Spach	0.73	50	5.7	24
22	Rhynchelytrum repens	0.33	49	5.9	73
23	Hevea brasiliensis	0.41	49	5.9	49
24	Trema tomentosa (Roxb.) H. Hara	0.49	47	5.5	50
25	Pinus kesiya var. langbianensis	0.42	39	5.5	49
26	Lasiococca comberi Haines H. S. Kiu	0.95	46	5.4	51

27	Broussonetia papyrifera*	1.4	37	5.1	48

Note that the "*" is representative of twig of this tree.

Table S2. Elemental analysis of 17 main coal types.

Types	IDs	Location	N%	C%	H%	O%	S%
Anthracite	34	Jining	0.51	75	3.4	6.2	0.29
	35	Yangcheng	0.39	75	3.5	5.1	0.00
	36	Liupanshui	0.73	80	3.5	4.5	0.20
	37	Menkou	0.57	85	3.1	5.5	0.00
	38	Xinxiang	0.61	86	3.3	5.2	0.00
	39	Chengzhou	0.65	77	3.3	5.0	0.09
	40	Yinchuan	0.18	91	4.3	3.8	0.00
Bituminous coal	41	Huainan	0.47	75	4.1	20	0.00
	42	Baitashan	0.30	68	3.9	29	0.00
	43	Longkou	1.0	65	4.8	27	0.19
	44	Baoji	0.25	68	4.0	21	0.00
	45	Lingshi	0.78	81	4.4	6.0	0.77
	46	Dazhou	0.44	76	3.3	6.9	0.30
	47	Shenmu	0.59	77	4.4	14	0.00
	48	Daqing	0.37	69	5.0	19	0.00
	49	Zibo	0.46	76	3.7	5.4	0.73
	50	Hailaer	0.58	64	4.7	30	0.00

Table S3. The EFs of 27 biomass burning and 17 coal combustion, and carbon contents of vehicle emission aerosols.

	Biomass burning		Anthracite combustion		Bituminous coal combustion		Vehicle emission	
	Avg	SD	Avg	SD	Avg	SD	Avg	SD
PM (g kg^{-1} fuel)	15	11	1.5×10^{-1}	8.9×10^{-2}	9.1×10^{-1}	6.5×10^{-1}	3.7 [a]	7.8 [a]
OC (g kg^{-1} fuel)	8.0	6.4	1.2×10^{-2}	4.5×10^{-3}	4.2×10^{-1}	3.3×10^{-1}	3.7×10^{-1} [a]	8.2×10^{-1} [a]
EC (g kg^{-1} fuel)	7.7×10^{-1}	3.4×10^{-1}	1.6×10^{-4}	1.4×10^{-4}	9.4×10^{-2}	1.9×10^{-1}	1.0×10^{-1} [a]	2.2×10^{-1} [a]
WSOC (μg C mL^{-1})	4.8	2.6	1.1	1.9×10^{-1}	3.2	3.7	2.6	1.8
MSOC (μg C mL^{-1})	8.5	10	1.1	1.0	25	26	2.5	1.1
WSOC/OC	0.50	0.15	0.66	0.18	0.13	0.08	0.45	0.11
MSOC/OC	0.62	0.18	0.47	0.14	0.80	0.20	0.56	0.25
OC/EC	16	32	145	99	21	28	3.0	1.5

Note: a, units (mg C m^{-3}).

Table S4. Mass absorption efficiency at 365 nm in different extracts from the three sources and comparison with the other studies.

	MAE_{365} (m^2 g^{-1} C)		Reference
Extracts	WSOC	MSOC	
Biomass burning	1.6 ± 0.55	2.3 ± 1.1	In current study
Anthracite combustion	1.3 ± 0.34	0.88 ± 0.74	
Bituminous coal combustion	2.0 ± 0.75	3.2 ± 1.1	
Vehicle emission	0.71 ± 0.30	0.26 ± 0.09	
Smoke particle from coal combustion	0.3−0.7 for bituminous coal, 0.9−1.0 for anthracite		(Li et al., 2018)
Rice straw burning	1.37± 0.23		(Park and Yu, 2016)
Pine needles burning	0.86± 0.09		
Sesame stems burning	1.38 ± 0.21		
Rice straw burning Corn straw burning Pine branch burning Coal smoke	1.23±0.33, 1.56±0.34, 0.79±0.22, 0.42±0.03, 0.8±0.03, respectively		(Fan et al., 2016)
Guangzhou $PM_{2.5}$	1.54 ± 0.16 (Winter) 0.73 ± 0.15 (summer)		(Yan et al., 2015)
Beijing $PM_{2.5}$	1.05±0.32		(Mo et al., 2018)
Beijing $PM_{2.5}$	1.79±0.24 (Winter), 0.71±0.2(summer)		(Cheng et al., 2011)
Nanjing $PM_{2.5}$	0.69(Spring),0.51(Summer), 0.70(fall),1.04(winter)		(Chen et al., 2018)
Guangzhou Total suspended particulate	0.81 ± 0.16		(Liu et al., 2018)

Table S5. Number of formulas in each compound category and the average values of elemental ratios, molecular weight (MW), double-bond equivalents (DBE) and aromaticity index (AI_{mod}) in MSOC from the six aerosol samples.

Sample IDs	Elemental composition	Number of formulas	MW_w	DBE_w	$AI_{mod,w}$	O/C_w	H/C_w	DBE/C_w
Musa	Total	2975	441.01	4.93	0.16	0.16	1.72	0.18
	CHO	1744	436.14	4.72	0.15	0.15	1.72	0.17
	CHON	1120	459.28	5.88	0.20	0.16	1.68	0.22
	CHOS	68	437.25	3.18	0.06	0.24	1.81	0.14
	CHONS	44	461.28	4.41	0.09	0.27	1.75	0.19
Hevea	Total	1527	400.39	6.95	0.29	0.22	1.50	0.30
	CHO	1255	393.74	7.78	0.32	0.22	1.42	0.34
	CHON	236	426.23	3.71	0.15	0.21	1.82	0.15
	CHOS	26	442.72	2.84	0.07	0.26	1.84	0.12
	CHONS	10	423.23	2.32	0.03	0.23	1.93	0.11
Anthracite	Total	1591	319.18	10.09	0.60	0.23	1.05	0.55
	CHO	491	304.11	9.67	0.55	0.19	1.09	0.51
	CHON	1000	321.49	10.50	0.63	0.24	1.02	0.58
	CHOS	59	383.70	4.32	0.21	0.32	1.65	0.23
	CHONS	41	361.72	4.39	0.33	0.39	1.64	0.28
Bituminous coal	Total	2037	343.07	13.19	0.61	0.13	0.93	0.59
	CHO	990	340.41	13.81	0.62	0.11	0.90	0.59
	CHON	839	345.09	12.43	0.61	0.16	0.97	0.59
	CHOS	195	360.61	11.06	0.52	0.23	0.98	0.56
	CHONS	13	396.51	10.71	0.48	0.26	1.10	0.53
Tunnel	Total	697	418.51	1.90	0.06	0.25	1.95	0.08
	CHO	358	393.28	3.21	0.13	0.19	1.81	0.14
	CHON	163	436.58	1.38	0.01	0.27	2.01	0.06
	CHOS	136	382.91	1.97	0.03	0.26	1.90	0.10

	CHONS	40	326.46	1.98	0.56	0.55	1.92	0.16
	Total	372	438.83	2.22	0.05	0.19	1.93	0.09
Vehicle	CHO	206	424.38	1.85	0.04	0.21	1.93	0.08
exhaust	CHON	143	449.71	2.21	0.06	0.18	1.95	0.09
	CHOS	17	467.89	3.75	0.08	0.13	1.80	0.14
	CHONS	6	429.35	5.25	0.12	0.22	1.66	0.23

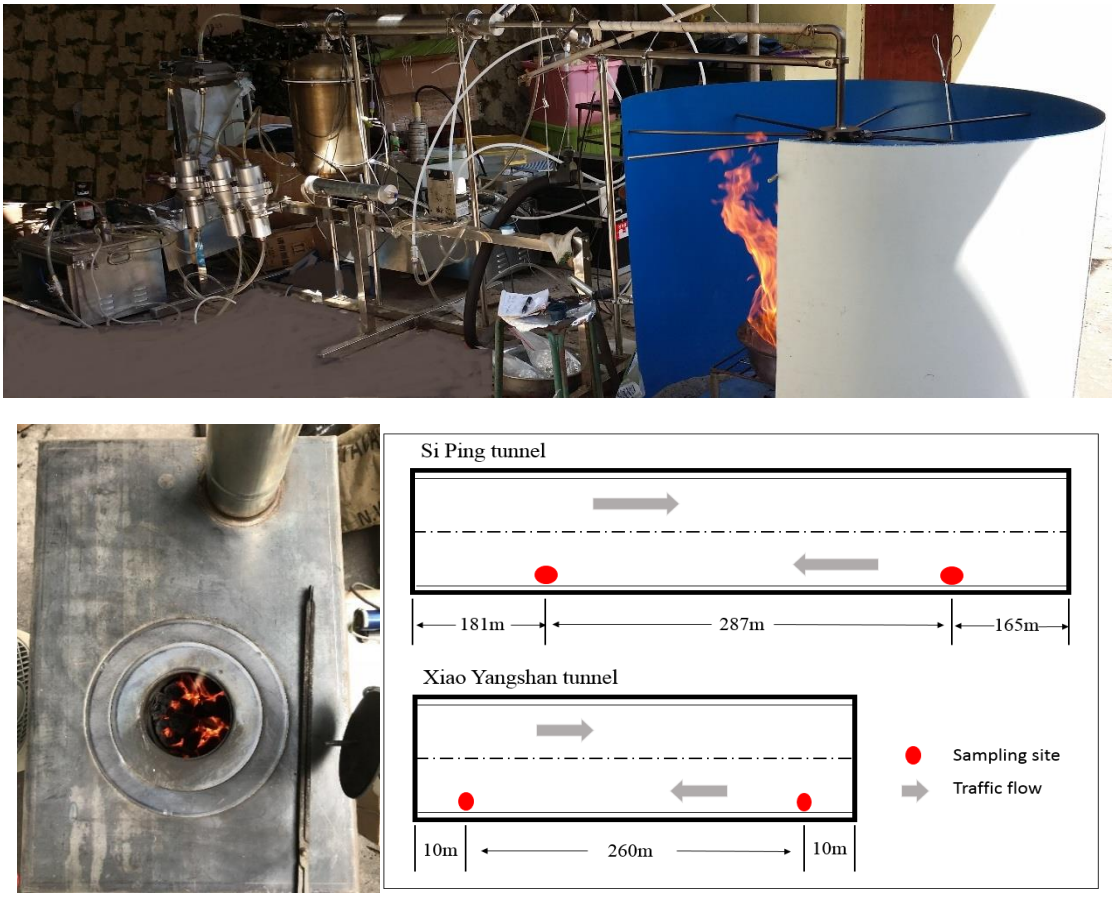

Figure S1. Experiments running in this work (biomass burning, coal combustion, and sampling schematic diagram of tunnel)

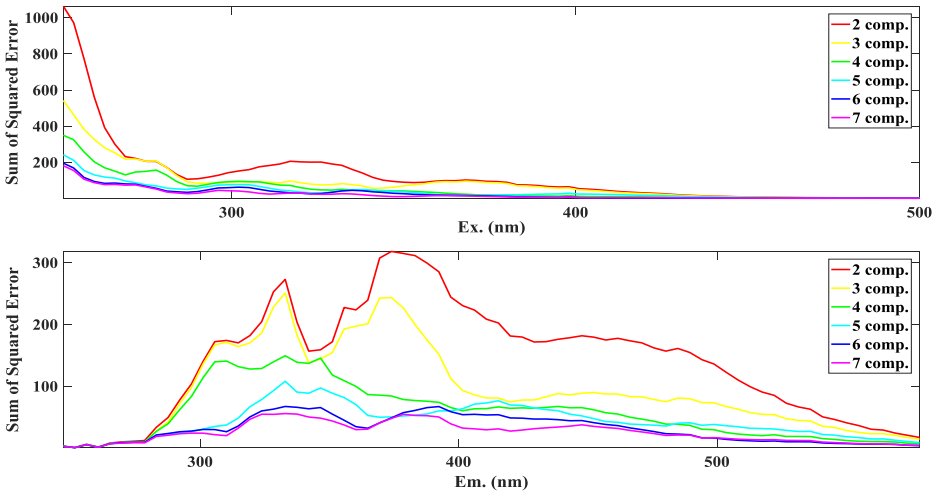

Figure S2. The residual analysis of excitation and emission wavelength of 2- to 7-components PARAFAC model for WSOC from the three sources

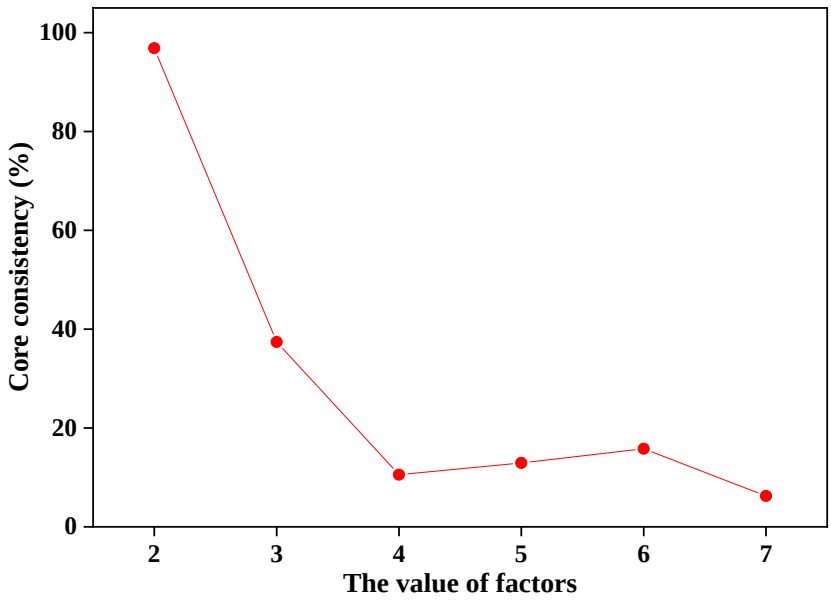

Figure S3. The core consistency of 2- to 7-component model for all EEM of WSOC from the three sources

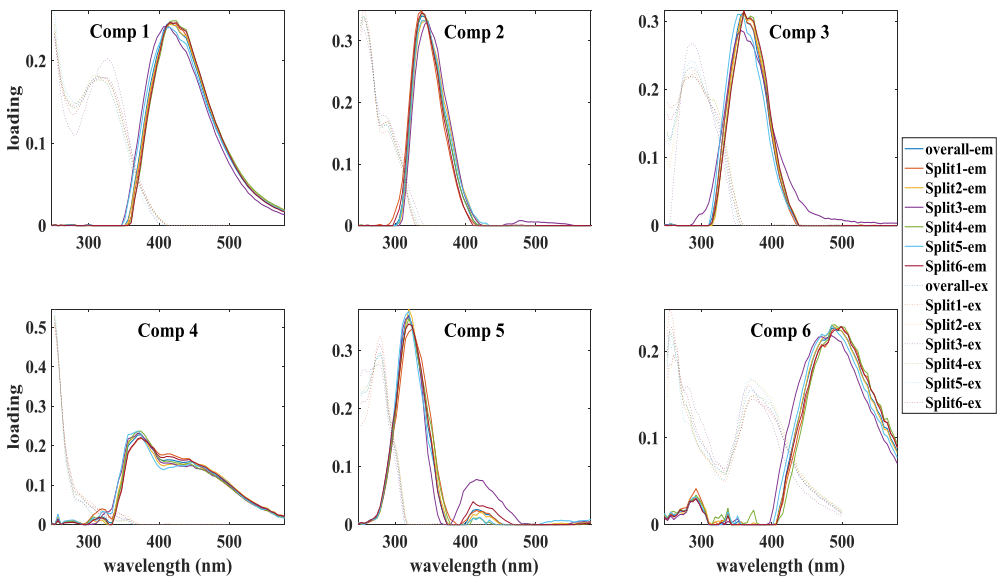

Figure S4. Split analysis of 6-component PARAFAC model with the split style '$S_4C_6T_3$' for all EEM of WSOC from the three sources

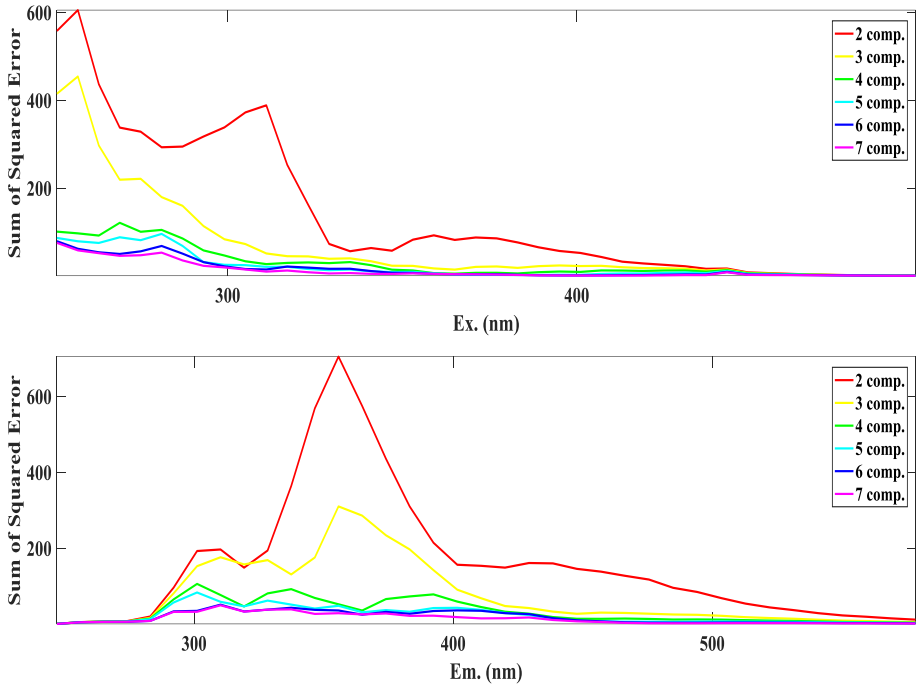

Figure S5. The residual analysis of excitation and emission wavelength of 2- to 7-components PARAFAC model for MSOC from the three sources

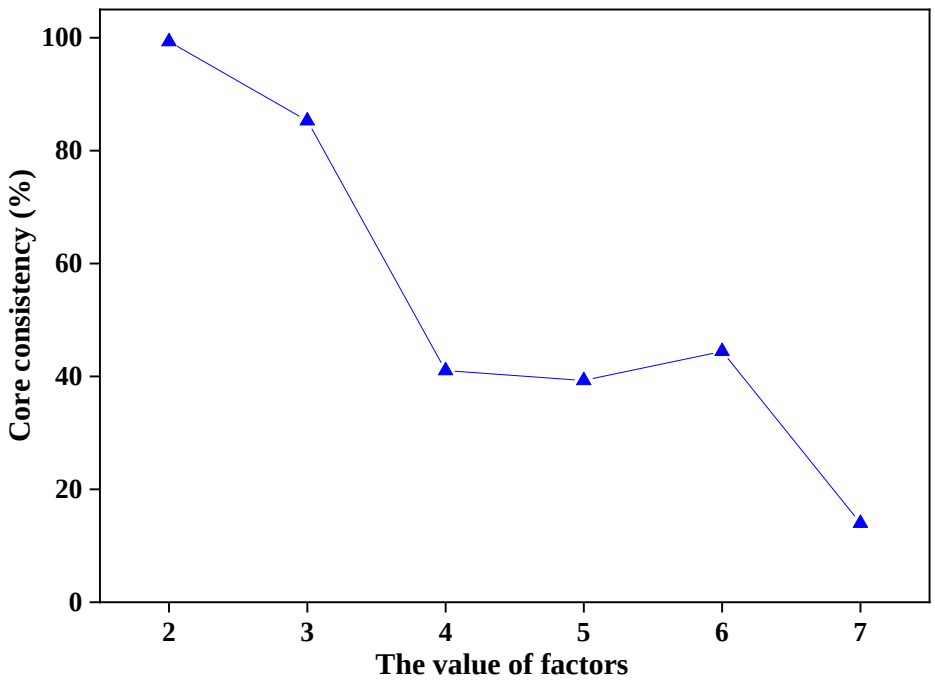

Figure S6. The core consistency of 2- to 7-component model for all EEM of MSOC from the three sources

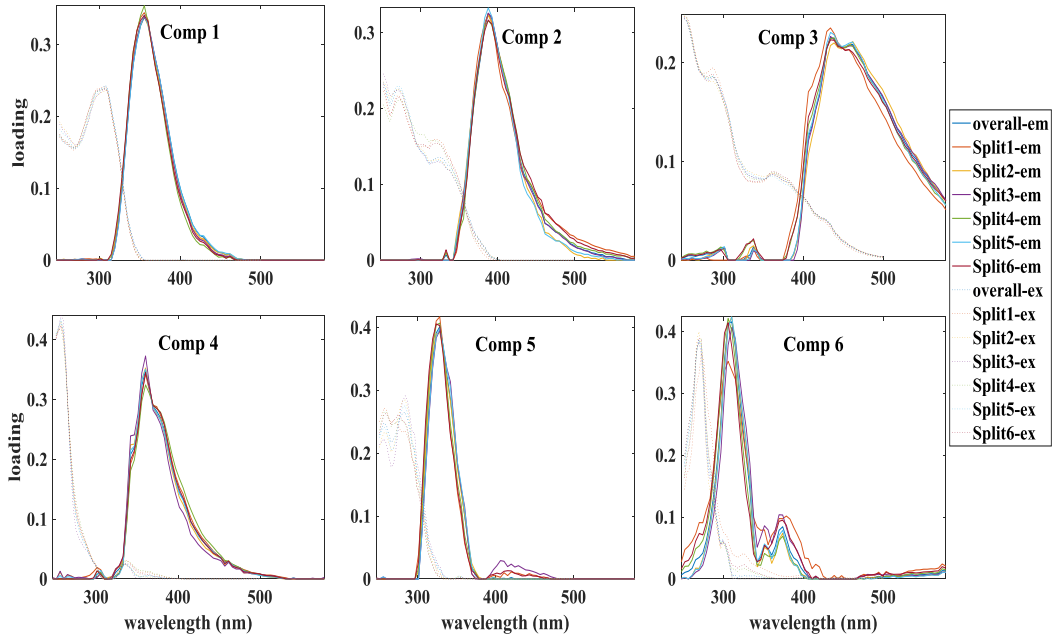

Figure S7. Split analysis of 6-component PARAFAC model with the split style '$S_4C_6T_3$' for all EEM of MSOC from the three sources

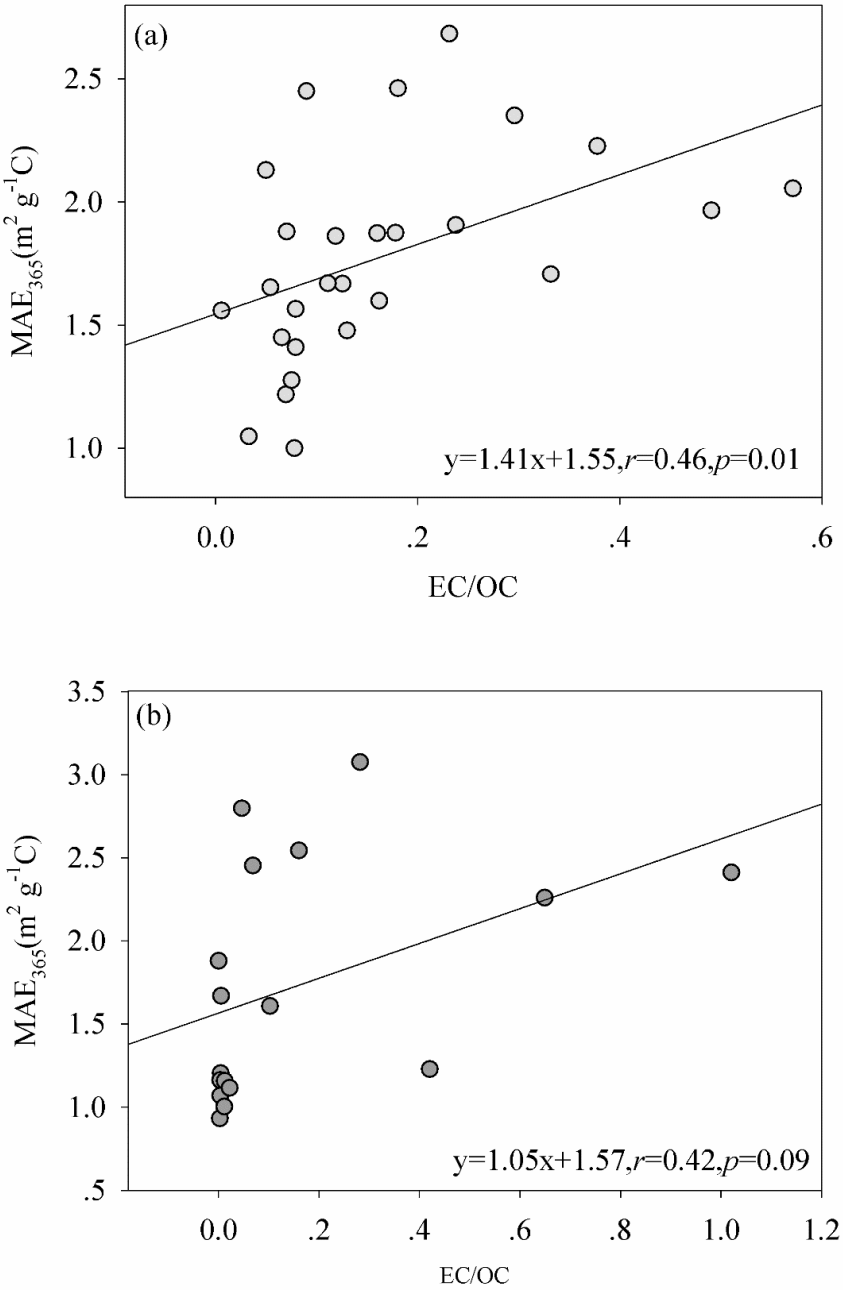

Figure S8. Linear regression coefficient of MAE_{365} of WSOC vs. EC/OC for (a) 27 BB aerosols, and (b) 17 CC aerosols

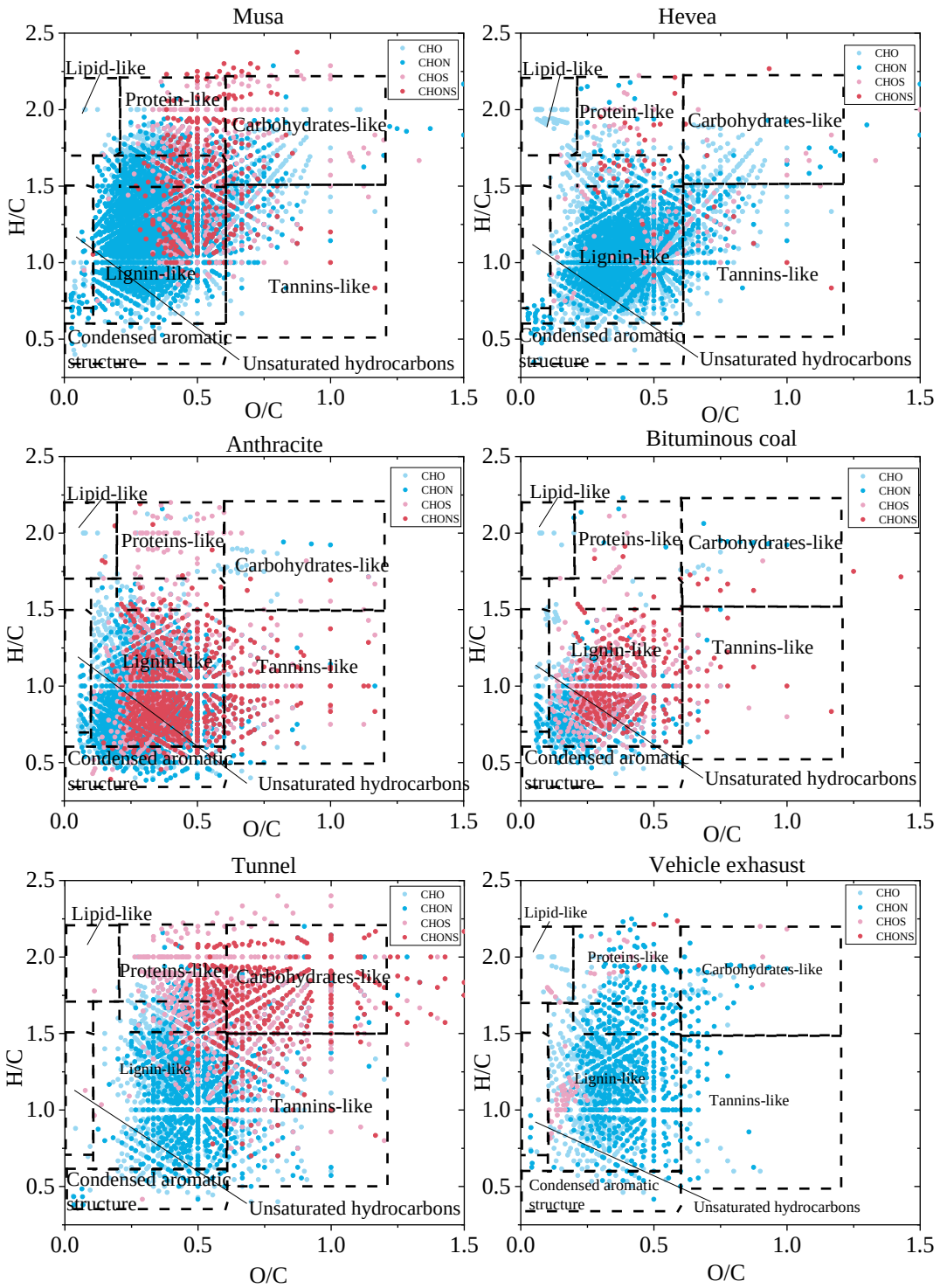

Figure S9. Ven diagrams of WSOC from the six aerosol samples. The different regions identified by O/C and H/C values were marked according to the previous study (Patriarca et al., 2018).

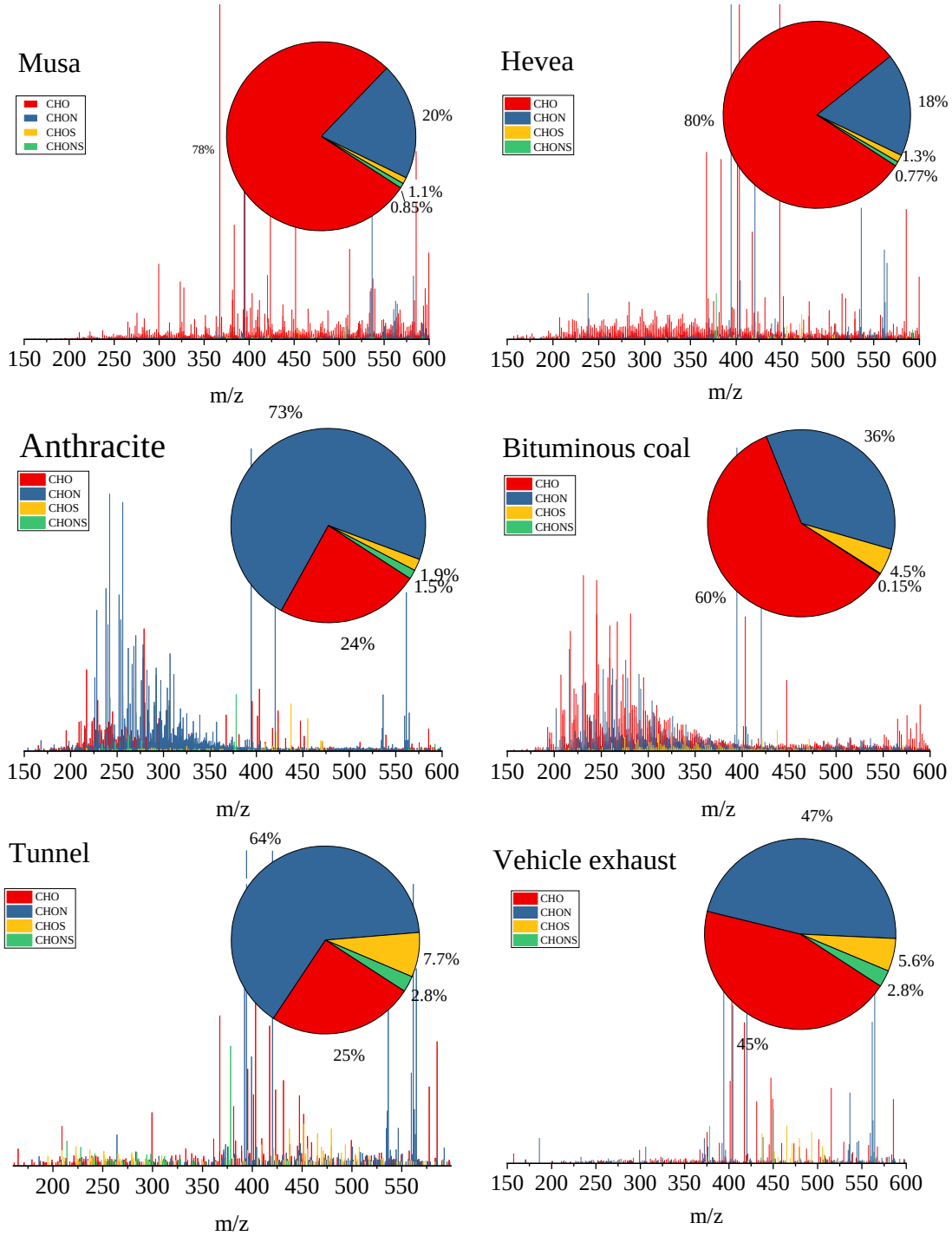

Figure S10. Negative ESI FT-ICR mass spectra of MSOC from the six aerosol samples. Different formula groups are color-coded. The six pie charts show the relative intensities of different formula groups in different samples.

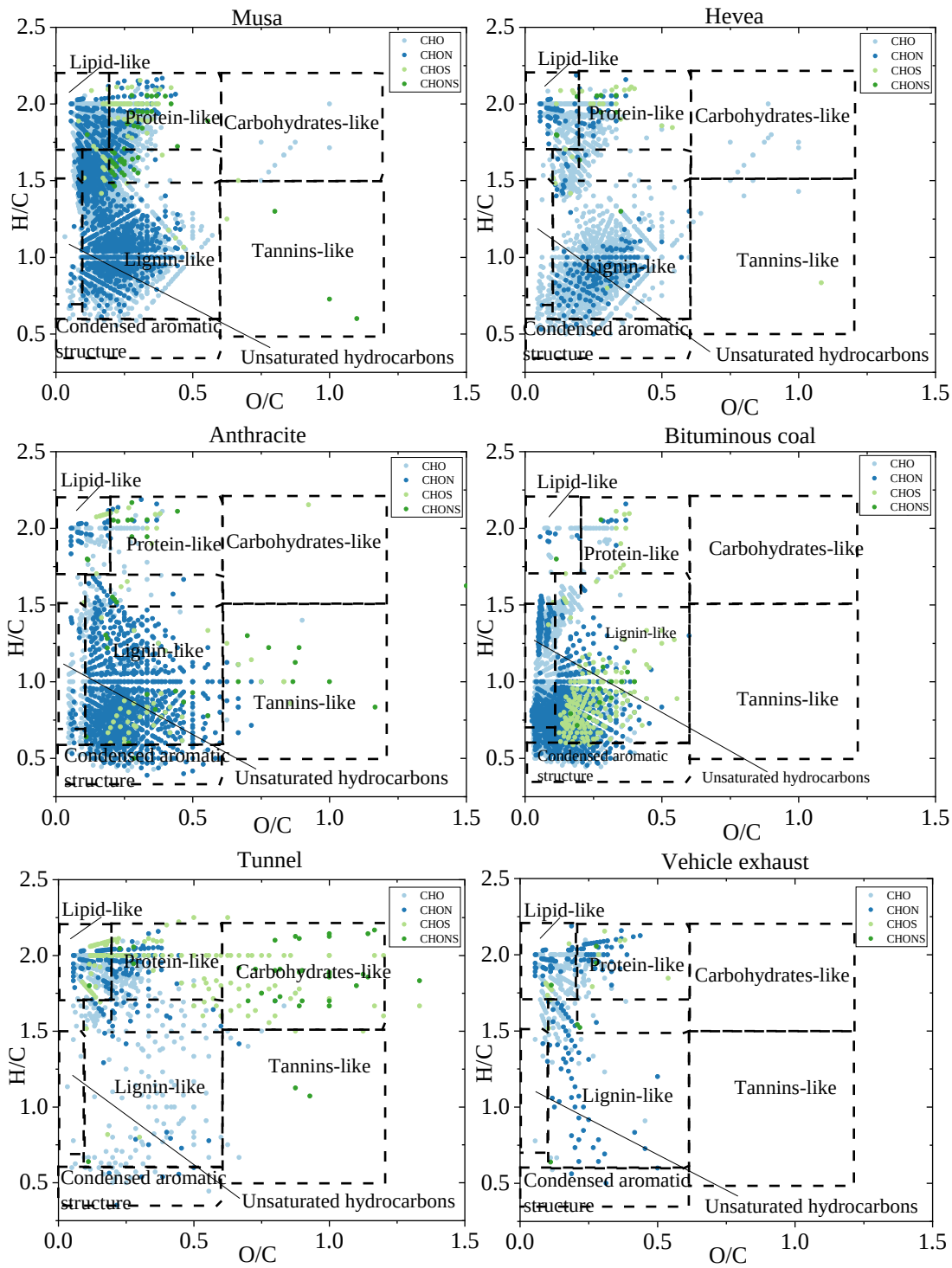

Figure S11. Ven diagrams of MSOC from the six aerosol samples. The different regions identified by O/C and H/C values are marked according to the previous study (Patriarca et al., 2018).

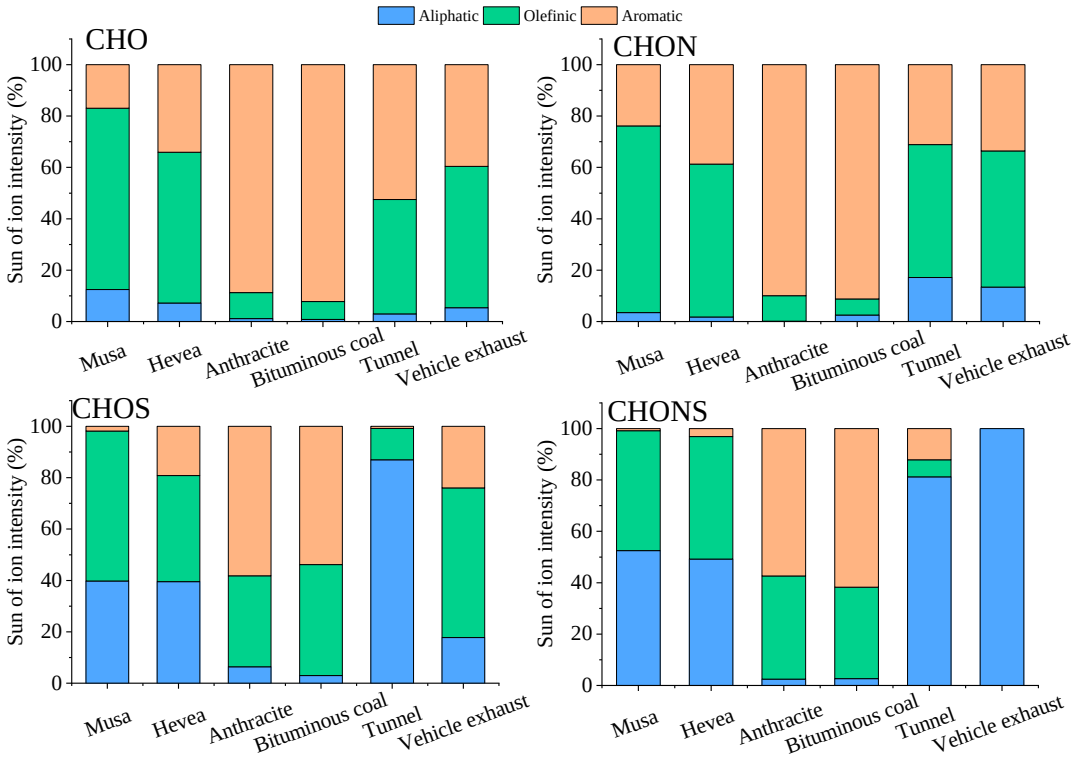

Figure S12. Sun of ion intensity fraction of aliphatic (AI_{mod}= 0), olefinic ($0<AI_{mod}\leq0.5$) and aromatic ($AI_{mod}>0.5$) in each compound class of WSOC from the six aerosol samples.

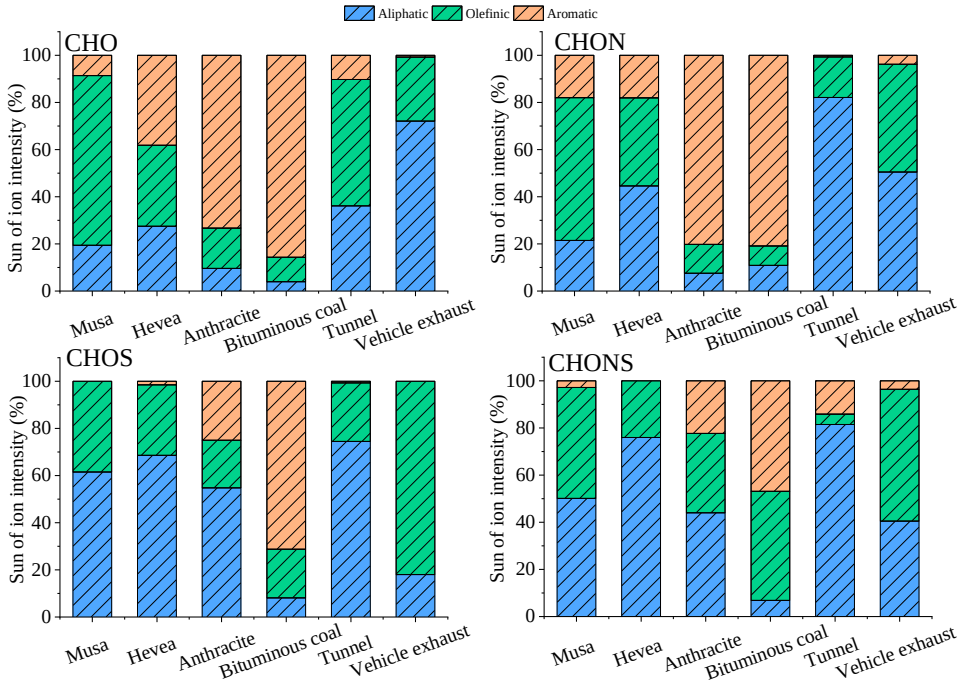

Figure S13. Sun of ion intensity fraction of aliphatic (AI_{mod}= 0), olefinic ($0<AI_{mod}\leq0.5$) and aromatic ($AI_{mod}>0.5$) in each compound class of MSOC from the six aerosol samples.

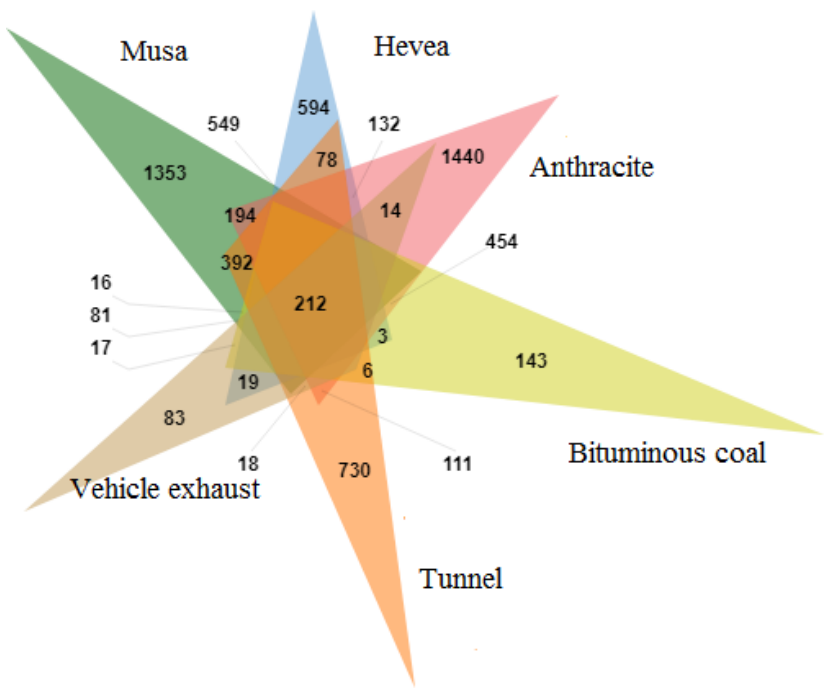

Figure S14. Venn diagrams for the relative distributions of all molecular formulas in WSOC from the six aerosol samples. The areas of overlap are the common elements in both, three, four, five or all six samples. The areas with no overlap are unique to that individual sample.

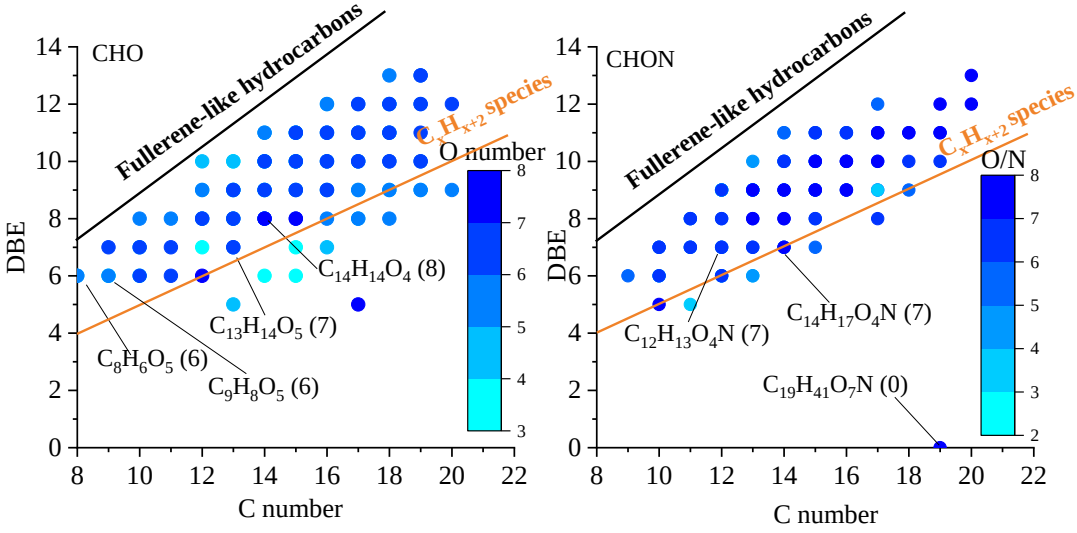

Figure S15. Plot of the DBE vs number of carbon atoms of molecules identified in WSOC detected in all the six aerosol samples. Lines indicate DBE reference values of linear conjugated polyenes C_xH_{x+2} with DBE=0.5×C, and fullerene-like hydrocarbons with DBE=0.9×C. The data points inside this region are potential BrC chromophores. Color bar denotes the O number and O/N for CHO and CHON, respectively.

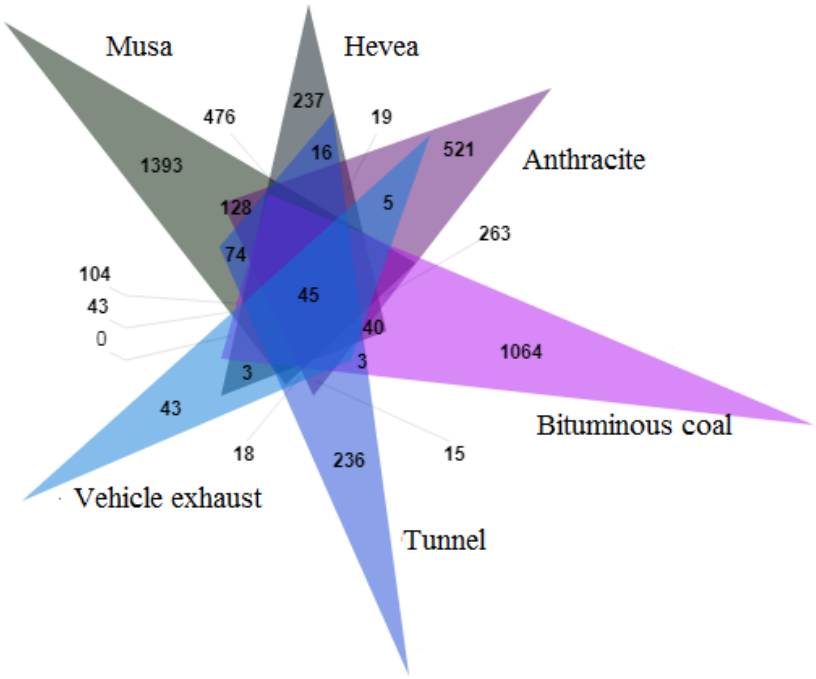

Figure S16 Venn diagrams for the relative distributions of all molecular formulas in MSOC from the six aerosol samples. The areas of overlap are the common elements in both, three, four, five or all six samples. The areas with no overlap are unique to that individual sample.

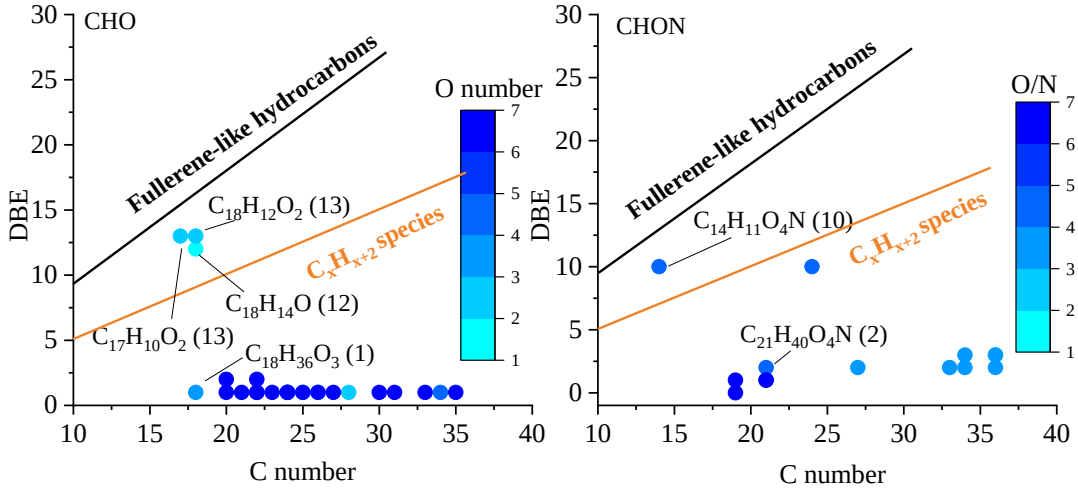

Figure S17. Plot of the DBE vs number of carbon atoms of molecules identified in MSOC detected in all the six aerosol samples. Lines indicate DBE reference values of linear conjugated polyenes C_xH_{x+2} with DBE=0.5×C, and fullerene-like hydrocarbons with DBE=0.9×C. The data points inside this region are potential BrC chromophores. Color bar denotes the O number and O/N for CHO and CHON, respectively.

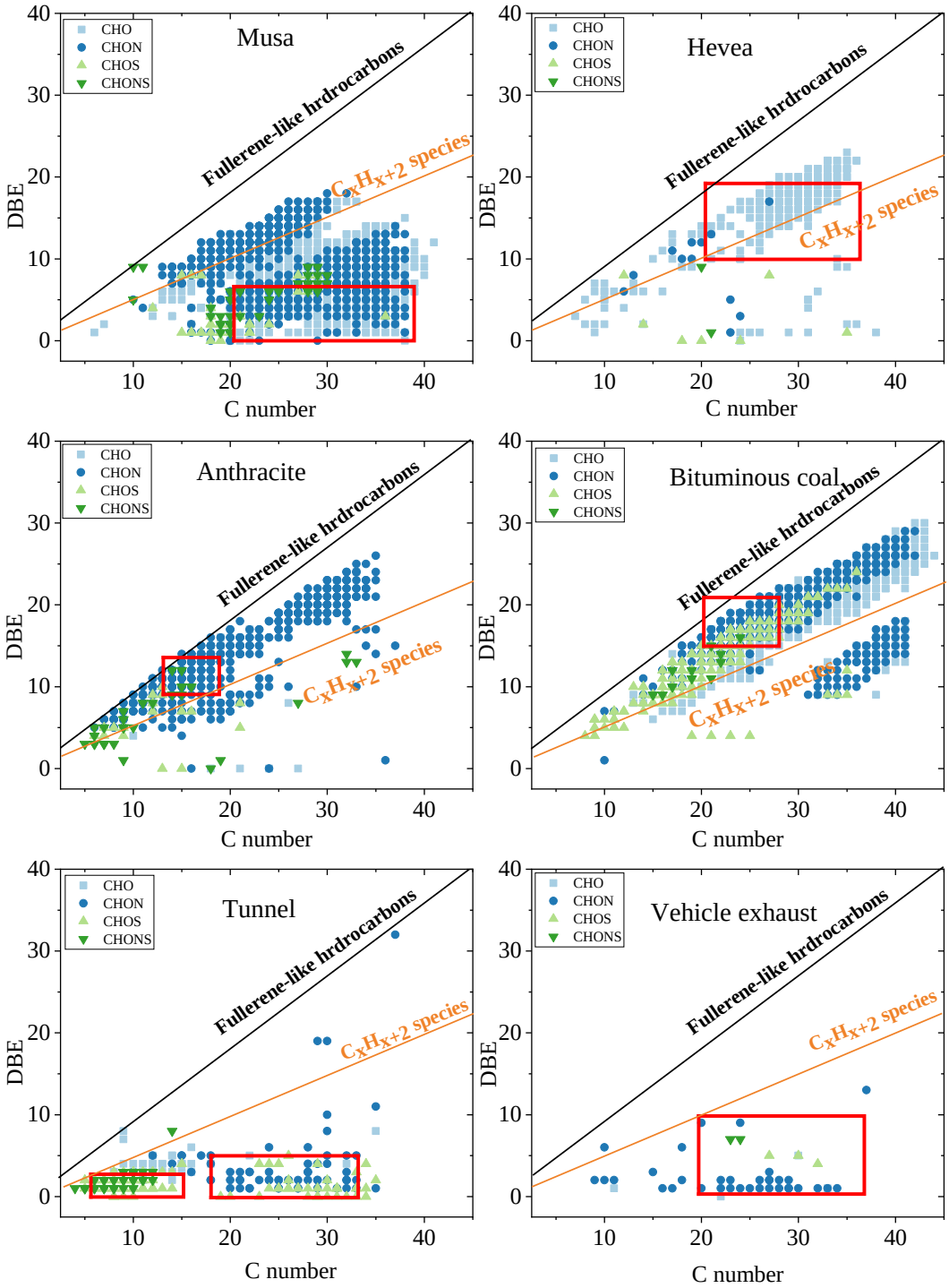

Figure S18. DBE vs C number for unique molecular compounds of MSOC from the six aerosol samples. Lines indicate DBE reference values of linear conjugated polyenes C_xH_{x+2} with DBE=0.5×C, and fullerene-like hydrocarbons with DBE=0.9×C. The regions marked by red box denoted the high intensities of compounds.

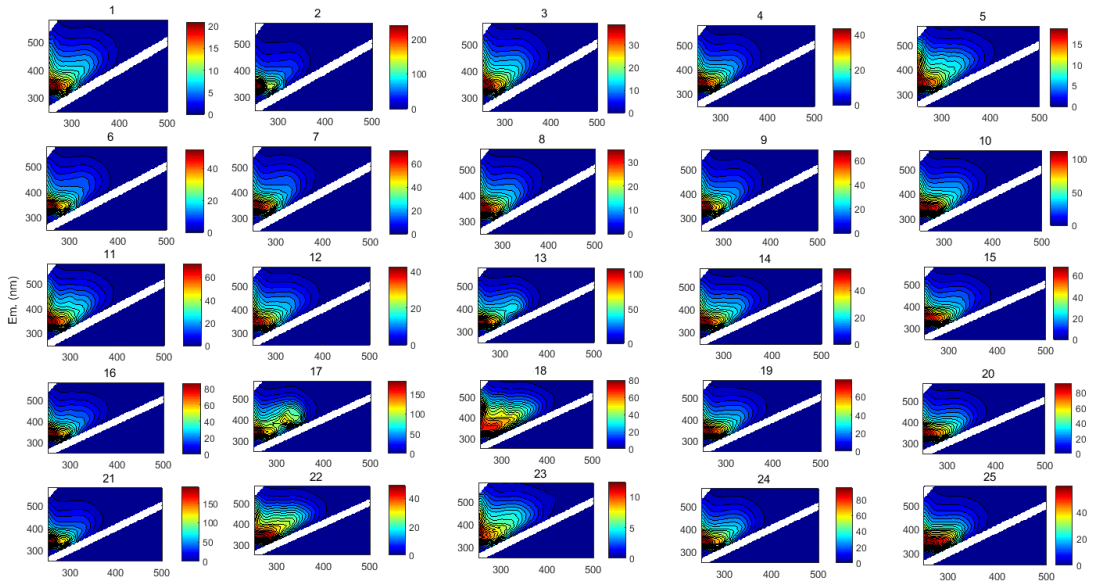

236

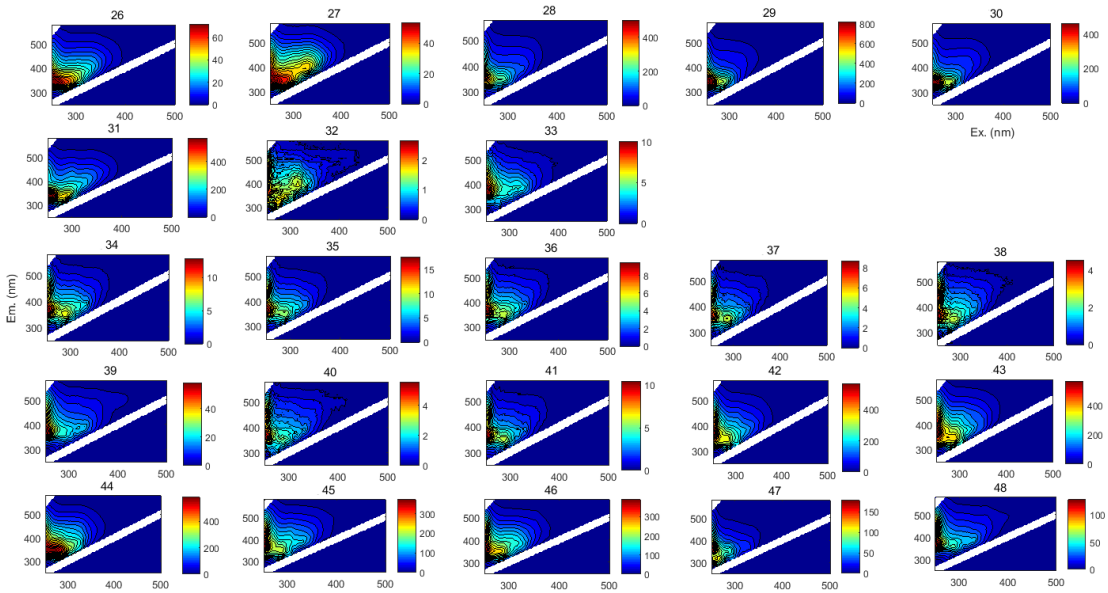

237

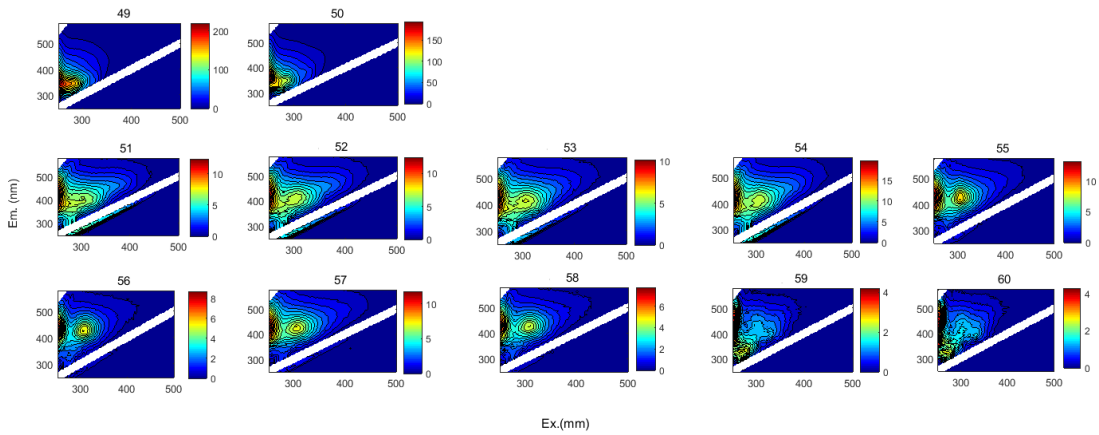

238

Figure S19. The EEMs spectra of WSOC from the three sources: IDs1−33 for BB aerosols, IDs34−50 for CC aerosols, and IDs51−60 for vehicle emissions.

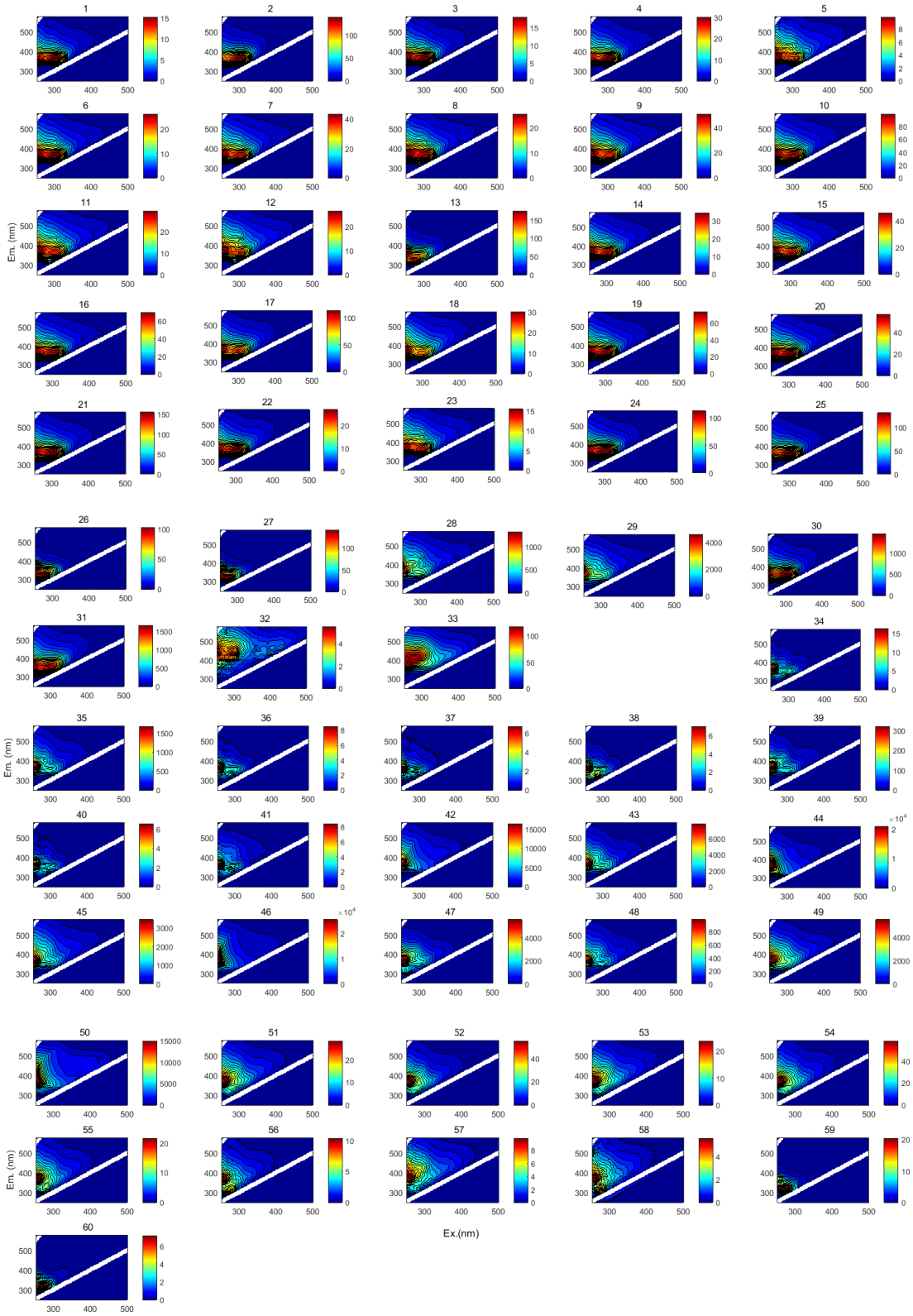

Figure S20. The EEMs spectra of MSOC from the three sources: IDs1−33 for BB aerosols, IDs34−50 for CC aerosols, and IDs51−60 for vehicle emissions.